Uplift Mechanisms of Pipes Buried in Sand

C. Y. Cheuk[1]; D. J. White[2]; and M. D. Bolton[3]

Abstract: Reliable design against upheaval buckling of offshore pipelines requires the uplift response to be predicted. This paper describes a model-scale investigation into the mechanisms by which uplift resistance is mobilized in silica sand, and illustrates how the observed mechanisms are captured in prediction models. A novel image-based deformation measurement technique has been used. The results show that peak uplift resistance is mobilized through the formation of an inverted trapezoidal block, bounded by a pair of distributed shear zones. The inclination of the shear zone is dependent on the soil density, and therefore dilatancy. After peak resistance, shear bands form and softening behavior is observed. At large pipe displacements, either a combination of a vertical sliding block mechanism and a flow-around mechanism near the pipe or a localized flow-around mechanism without surface heave is observed, depending on the soil density and particle size.

DOI: 10.1061/(ASCE)1090-0241(2008)134:2(154)

CE Database subject headings: Buried pipes; Soil deformation; Sand; Uplift resistance; Particle size; Imaging techniques.

Introduction

Upheaval Buckling

Failure of an oil or gas pipeline has serious economic and environmental consequences. One key failure mode associated with subsea pipelines is thermal buckling. To ease the flow, pipelines operate at high temperature (typically 160 °C) and pressure (typically 70 MPa). These operating conditions cause axial thermal expansion which is restrained by friction at the soil–pipe interface and the end connections. Axial compressive forces as high as ~1.5 MN can be generated leading to a vulnerability to buckling in either the vertical or lateral direction (Hooper et al. 2004). High passive resistance resists buckling in the lateral direction. The weakest mode of buckling is in the vertical plane. The term upheaval buckling is used to describe this failure mode, leading to protrusion of the pipeline through the soil cover, and in extreme cases, bending failure.

Design Challenges

The design of a buried pipeline requires the minimum depth of soil cover that will provide sufficient uplift resistance to be determined. Burial represents a significant portion of the total construction cost, which is highly dependent on the burial depth, and should therefore be minimized while maintaining adequate safety. The uplift resistance must be mobilized at a sufficiently small pipe displacement to avoid buckle initiation. Where the pipeline has any overbend, the thermally induced axial force must be balanced by the mobilized uplift resistance. The form of the uplift load-displacement relationship affects whether a deformed equilibrium position is reached.

The current design approaches for predicting peak uplift resistance from soil type and cover depth are based on simple rigid block mechanisms, checked against measurements of uplift resistance in model tests. The aim of the research described in this paper is to examine the soil deformation during pipe uplift, to allow more robust verification of current prediction methods for the chosen soil type or materials with similar properties. A series of four model tests in which the soil deformation during pipe uplift is observed by image analysis are described. The tests were conducted in a transparent-sided plane-strain calibration chamber at approximately half-scale. An image analysis technique based on particle image velocimetry (PIV) combined with close range photogrammetry (White et al. 2003) has been used to track the soil movement at many thousands of points within the model without recourse to intrusive target markers. Focus is placed on the effect of particle size and soil density for the uplift response.

Previous Investigations into Pipe Uplift

Load–Displacement Response

Many previous model tests have been conducted to investigate uplift resistance and the corresponding failure mechanism (e.g. Trautmann et al. 1985; Ng and Springman 1994; Bransby et al. 2001; White et al. 2001; Chin et al. 2006; Schupp et al. 2006). Two distinct forms of response have been identified depending on the volumetric behavior of the soil (Schaminée et al. 1990). For contractive soil, either due to low relative density or high confining stress, the uplift resistance increases monotonically with the pipe displacement. In dilatant conditions a stiff initial response up to peak resistance is followed by softening.

[1]Assistant Professor, Dept. of Civil Engineering, The Univ. of Hong Kong, Pokfulam, Hong Kong (corresponding author). E-mail: cycheuk@hkucc.hku.hk

[2]Senior Lecturer, Centre for Offshore Foundation Systems, Univ. of Western Australia, Crawley, Australia.

[3]Professor of Soil Mechanics, Dept. of Engineering, Univ. of Cambridge, Cambridge, UK.

Note. Discussion open until July 1, 2008. Separate discussions must be submitted for individual papers. To extend the closing date by one month, a written request must be filed with the ASCE Managing Editor. The manuscript for this paper was submitted for review and possible publication on March 21, 2006; approved on April 10, 2007. This paper is part of the ***Journal of Geotechnical and Geoenvironmental Engineering***, Vol. 134, No. 2, February 1, 2008. ©ASCE, ISSN 1090-0241/2008/2-154–163/$25.00.

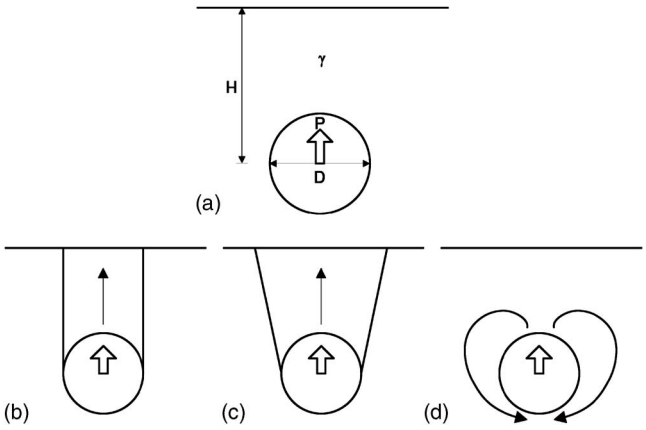

Fig. 1. Uplift mechanisms of buried pipes in sand: (a) Problem geometry; (b) sliding block with vertical slip surfaces; (c) sliding block with inclined slip surfaces; and (d) flow around

Failure Mechanisms

The geometry of a buried pipe is defined in Fig. 1(a). Previous observations suggest that the uplift mechanism involves a sliding block bounded by a pair of shear bands [Fig. 1(b)]. The inclination of the shear bands is close to the soil dilation angle [Fig. 1(c)] (Ng and Springman 1994; White et al. 2001). Vanden Berghe et al. (2005) broadly confirmed this mechanism through finite element analyses. For very loose sand, localized shear with a flow-around mechanism was observed in model tests conducted by Bransby et al. (2001). This mechanism was also observed in an initially dense model beyond peak resistance (White et al. 2001), and has been predicted numerically for very loose sand, with a dilation angle of −10° (Vanden Berghe et al. 2005). However, Bransby et al. (2001) pointed out that the peak uplift load is mobilized at a very small displacement—typically ~1% of the pipe diameter—and previous work has not been able to identify the particular deformation mechanism operative at this early stage. In this study, new image analysis techniques have been used to capture the mechanism relevant to peak resistance.

Mobilization Displacement

Trautmann et al. (1985) expressed the peak mobilization displacement, δ_P, as a function of the embedment depth, H. The measured values of δ_P/H range between 0.5 and 1.5% with some systematic but scattered variation with embedment ratio H/D, suggesting that δ_P/D may be an equally applicable normalization. Bransby et al. (2001) identified a similar mobilization displacement of $\delta_P/H=0.5\%$ from finite element analyses that showed no influence of pipe diameter on δ_P. In centrifuge model tests that extended to a greater embedment, Dickin (1994) reported that the ratio δ_P/D increases from ~1 to ~15% for dense sand, and from ~1 to ~40% for loose sand, as the embedment ratio H/D increases from 1 to 8. These data are better normalized by cover depth with δ_P/H increasing from ~1 to ~2% in dense, and from ~1 to ~5% in loose sand, over this range of H/D.

Prediction Models for Peak Resistance

Various models have been proposed for the calculation of peak uplift resistance based on the mechanisms observed in previous model tests. Key prediction methods and the underlying assumptions are listed in Table 1. All methods assume that tension cannot be sustained between the pipe invert and the soil, allowing a gap to open without resistance.

Vertical Slip Limit Equilibrium Solution

The simplest mechanism is a limit equilibrium solution known as the vertical slip model [Fig. 1(b)]. Uplift resistance is due to the shear resistance along the vertical slip surfaces and the weight of the lifted soil block. An earth pressure coefficient, K, must be assumed, in order to link the geostatic vertical stress to the normal stress on the shear planes. This limit equilibrium solution has been used by Schaminée et al. (1990) to backanalyze a program of model tests, finding values of $K\tan\phi$ in the range 0.3–0.5 (Table 1).

Inclined Plane Upper Bound Solution, $\phi=\psi$

Vermeer and Sutjiadi (1985) describe an upper bound mechanism—requiring normality to be obeyed (i.e., $\phi=\psi$)—with straight shear bands extending to the soil surface [Fig. 1(c)]. For a purely frictional soil obeying normality, the uplift resistance is equal to the weight of the trapezoidal soil block as the dissipation within the soil is zero. The resulting resistance is identical to the vertical slip model for the case of $K=1$, and has been used by Ng and Springman (1994) to backanalyze tests using sand and rockfill (Table 1).

Limit Equilibrium Solutions with Inclined Planes, $\phi\neq\psi$

Vermeer and Sutjiadi (1985) suggest that the unconservative nature of a formal upper bound solution—as ψ is usually less than ϕ—could be avoided using Rowe's stress-dilatancy flow rule to infer a lower angle of dilation than friction (Rowe 1962; Bolton 1986). To calculate the resistance on the shear planes, it is assumed that the vertical stress on these planes arises only from self-weight. This assumption that vertical stresses remain geostatic is inconsistent with the increase in vertical stress above the pipe due to the uplift force. However, it does lead to a simple expression for peak shear stress on the inclined planes (Table 1).

White et al. (2001) suggest an alternative limit equilibrium

Table 1. Prediction Models for Peak Uplift Resistance

Reference	Prediction model	Assumed mechanism
Schaminée et al. (1990)	$P=\gamma' HD+\gamma' H^2 K\tan\phi$	Vertical slip surfaces
Ng and Springman (1994)	$P=\gamma' HD+\gamma' H^2\tan\phi_{max}$	Sliding block with inclined failure surfaces
Vermeer and Sutjiadi (1985)	$P=\gamma' HD+\gamma' H^2\tan\phi_{max}\cos\phi_{crit}$	Sliding block with inclined failure surfaces
White et al. (2001)	$P=\gamma' HD+\gamma' H^2\tan\psi$ $+\gamma' H^2(\tan\phi_{max}-\tan\psi)[(1+K_0)-(1-K_0)\cos 2\psi/2]$	Sliding block with inclined failure surfaces

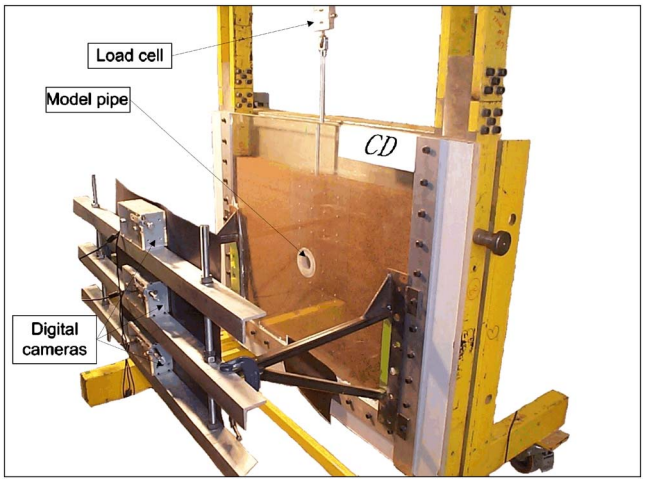

Fig. 2. Model test chamber for pipe uplift test

solution based on the same mechanism (Table 1). Instead of assuming that the vertical stress on the slip surfaces remains unchanged during uplift, it is assumed that the normal stress is constant. This assumption reduces the disparity between the assumed vertical stress at the end of the shear planes near the pipe crown, and the vertical stress created by the uplift force P. Bolton's (1986) flow rule, which is operationally indistinguishable to Rowe's stress-dilatancy, is used to find angles of friction and dilation linked to relative density and stress level.

Summary of Mechanisms

Each mechanism makes certain assumptions about the deformation pattern at peak uplift resistance. Where normality is violated, both angles of friction and dilation are required, and some assumption must be made regarding the shearing resistance along the failure planes. The model tests described in this paper aim to establish the realism of these assumptions.

Experimental Arrangement

Equipment

The test chamber has inside dimensions of 75.5 mm $\times$ 1,000 mm $\times$ 835 mm (Fig. 2). Two glass plates on the inner walls of the chamber reduce side friction. The model pipe, of diameter 100 mm, was made from a hollow brass tube with polytetra-fluroethylene caps to reduce friction, and fit flush between the sides of the chamber. The smooth surface of the model pipe closely mimicked the field situation in which the pipeline is normally coated with a polymer. Black dots on the pipe end provided artificial "texture" allowing tracking by image analysis. A jointed aluminum rod connected the pipe to a vertical actuator via a load cell.

Uplift movement was controlled by an actuator mounted on the calibration chamber. Two digital cameras viewed each experiment, controlled by PC via a USB connection. Further details of the experimental set-up are described by Cheuk (2005).

Test Materials

Uniform silica sands of two different particle sizes were used. Leighton Buzzard (LB) silica sand has been widely used in previous research and its mechanical behavior is well documented (e.g., Stroud 1971; Lee 1989). Fraction A LB sand [Fig. 3(a)] has a D_{50} of 2.24 mm. The maximum and minimum void ratios were measured to be 0.83 and 0.55, respectively. D_{50} of the finer Fraction D LB sand [Fig. 3(b)] is 0.28 mm, which is 8 times smaller than Fraction A. The maximum and minimum void ratios of this fine sand were found to be 1.01 and 0.68, respectively, which are comparatively higher than those of Fraction A due to its greater angularity (Mak 1983). Direct shear box tests revealed that the two sands share a critical state friction angle, ϕ_{crit}, of 32°. This suggests that, despite the possible differences in shapes, angularity and surface texture of the two types of sand, the influence on engineering properties, especially the frictional characteristics, is minimal.

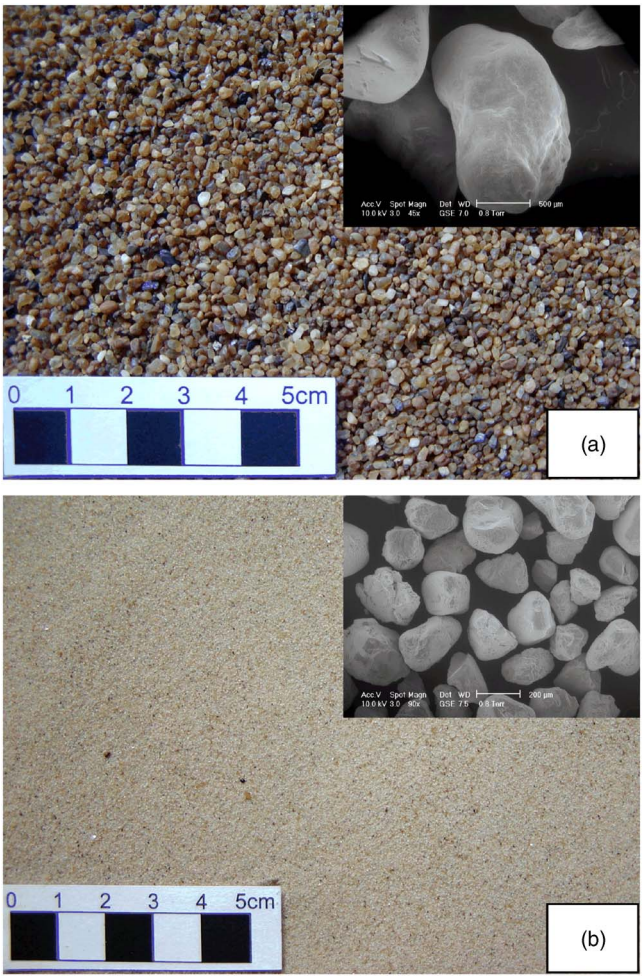

Fig. 3. Leighton Buzzard silica sands used in this study: (a) Fraction A; (b) Fraction D

The interface friction between the sands used in this study and the glass walls is assumed to lie in the range of 10–15° based on previously reported values from others: White (2002) measured a value of 11° in direct shear box interface tests on Fraction B silica sand (D_{50}=0.84 mm) sliding on a glass plate and Cousens (1980) reported a value of 14° for a finer fraction (D_{50}=0.55 mm) of the same silica sand. This low interface friction, relative to the friction angle of the soil, together with the close fit of the model pipe within the chamber, ensures that the soil movement observed at the window is the same as that present through the cross section. This assumption has been confirmed by the soil movement mea-

Table 2. Summary of Test Conditions and Key Results

Test		CD	CL	FD	FL
Soil properties	Mean particle diameter, D_{50}	2.24	2.24	0.28	0.28
	Soil density, ρ_s (kg/m^3)	1,687	1,532	1,551	1,386
	Relative density, I_D (%)	92	36	92	30
	Friction angle at critical state, ϕ_{crit} (deg)	32	32	32	32
	Relative dilatancy index, I_R[a]	4	2.1	4	1.58
	Peak dilation angle, ψ_{peak}[a] (deg)	25	13.1	25	9.9
	Peak angle of friction, ϕ_{peak}[a] (deg)	52	42.5	52	39.9
Results	Peak uplift force, P (N)	127	82	136	114
	Pipe displacement at peak, δ_P (mm)	2.95	2.86	3.10	3.02

Note: CD=Corase, dense; CL=Corase, loose; FD=Fine, dense; and FL=Fine, loose.

[a]Calculated following Bolton (1986).

sured manually at the soil surface, which is uniform across the width of the chamber. Nevertheless, due to the frictional resistance at the interface the stress distribution above the pipe would be different compared to true plane strain conditions. This discrepancy may lead to a slightly higher uplift resistance.

Model Preparation

Overhead transparency sheets printed with a grid of black dots were fixed inside the chamber window. These control markers were used to convert the displacements calculated in image-space into object-space coordinates, eliminating image distortion. A pneumatic sand pouring system was used to prepare a uniform soil model. By adjusting the travel speed, drop height, and flow rate of the pourer, sand layers of different densities are obtained.

The model chamber was filled up by sand until the position corresponding to the center of the model pipe. A cavity was created by carefully removing sand particles and the model pipe was installed. Pouring continued until a cover depth, H, of 300 mm was reached (Fig. 2). Trial tests were conducted to examine the consistency of the model preparation process. The soil density varied by ±1.5% ensuring repeatability.

Test Program

A series of four tests involving two grain sizes and two relative densities (~30 and ~90%) was conducted (Table 2). The initial stress level of the soil at the pipe level is ~4 kPa, which has been used to estimate the dilation angle of the soil based on Bolton's (1986) correlations.

Typical offshore pipelines have an outer diameter ranging from 0.15 to 0.4 m (from 6 to 16 in.), buried at a depth of 0.5–1 m. The selected cover depth ratio, H/D, of 3 represents a typical prototype, albeit with the dimensions scaled down by a factor of ~2. Due to this down scaling, the overburden stress at the pipe level would be approximately half compared to a full-scale model. However this reduction in stress level is rectified by the use of dry sand, which has approximately twice the effective unit weight compared to its saturated state. The pulling speed in all the four tests was 10 mm/h, with digital images captured at intervals of 90 s or less (corresponding to ~250 μm of pipe movement, or less).

Image Analysis Technique

In order to quantitatively study the failure mechanism, it is necessary to calculate the displacement field in the deforming soil. The technique of PIV has been used in combination with close range photogrammetry (White et al. 2003).

PIV is a measurement technique that was originally developed in the field of experimental fluid mechanics to recover instantaneous velocity fields from photographs of seeded flow. PIV calculates the displacement (or instantaneous velocity) field between an image pair by dividing the initial image into a mesh of interrogation patches, which are effectively square regions of pixels whose brightness distribution characterizes the soil at that point. The displacement of each of these interrogation patches is calculated by correlation with a larger search patch from a subsequent image (White et al. 2003). The highest peak in the normalized correlation plane indicates the best match between the interrogation and search patches, revealing the displacement of the interrogation patch.

The precision of PIV is dependent on the size of the interrogation patch, and is typically 1/20th of a pixel in geotechnical applications (White et al. 2005). The subpixel precision is achieved by cubic spline interpolation, and has been validated by calibration experiments in which known displacements are imposed and checked against PIV predictions (White et al. 2003). In this study the image scale varied in the range 0.09–0.11 mm/pixel, which leads to an object-space precision of 5 μm.

The outcome of the PIV analysis is a displacement field in image-space (pixel) coordinates. These results are converted into object-space coordinates by means of image calibration. The relative coordinates of the control markers were established prior to the experiment. Multiple-threshold centroiding (Take 2003) was used to establish the image-space coordinates of these markers, from which the parameters governing the transformation between image and object spaces were found. This transformation process is based on the principles of close range photogrammetry, and takes into account several effects that can cause distortions in digital images, including fish eye, refraction, and noncolinearity of the normals to the image and object planes (White et al. 2003).

Load–Displacement Response

A calibration test was conducted to determine the frictional force exerted on the ends of the model pipe against the walls of the model chamber. The measured uplift force was constant and equal to 10±2 N and the mean value, 10 N, has been subtracted from the measured uplift force to obtain the net uplift force.

Fig. 4 shows the variation of net uplift force with pipe displacement for all four tests; peak values are shown in Table 2. All tests exhibited a sharp increase in uplift resistance in the first 0.5 mm, and mobilized a peak at 3–4 mm, irrespective of density and grain size. The maximum net uplift resistance in the two

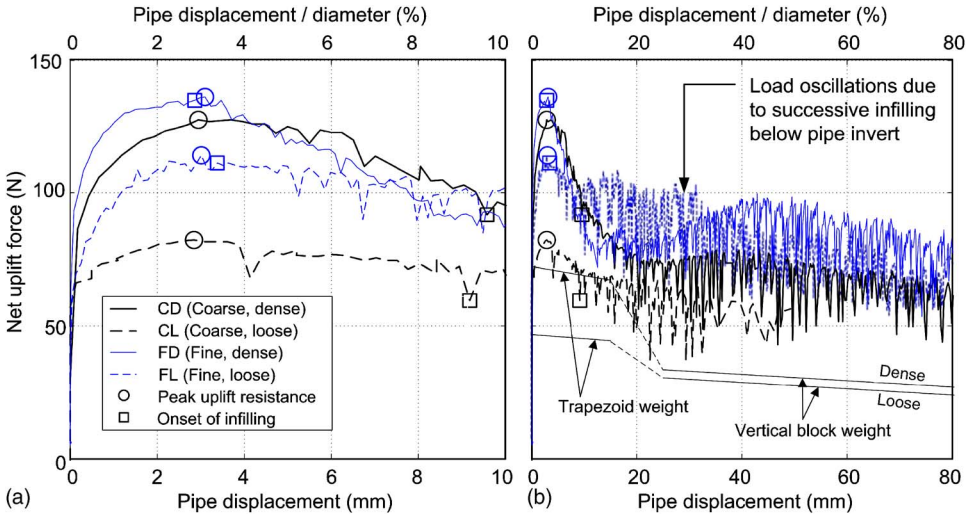

Fig. 4. Load–displacement response during pipe uplift: (a) δ=0–10 mm; (b) δ=0–80 mm

dense tests (CD and FD) corresponds to 16.8 and 18.0 kPa acting vertically over the projected pipe area. These values compare with at-rest vertical stresses of 5.0 and 4.6 kPa at a depth of 300 mm, respectively.

In the loose tests (CL and FL) peak stresses of 10.9 and 15.1 kPa were recorded in coarse and fine sand, respectively. The higher resistance encountered in the fine sand could be partly attributed to increased friction as the small sand particles clogged the interface between the pipe ends and the chambers walls. Chin et al. (2006) compared the peak uplift resistance obtained from a number of studies, including the test data reported herein. Their comparison suggests that the uplift forces measured in this study are in good agreement with measurements made elsewhere.

A softening response was observed in all tests with a greater reduction (>40%) in uplift resistance observed in dense soil. No trend links the ultimate resistance and particle size or soil density. Significant oscillations of up to 20 N were observed postpeak, similar to observations by Trautmann et al. (1985) and Dickin (1994). Examination of the images revealed that these jumps coincided with miniature slope failures as soil fell around the pipe periphery into the cavity below (Fig. 5).

These slope failures have significant implications for the upheaval buckling behavior of the pipe. During cyclic thermal loading, the infilling at the pipe invert triggers upward racheting. If infilling occurs during a cycle of uplift, the pipeline cannot return to the original configuration upon cooling. This irrecoverable movement enlarges any overbend in the pipe, leading to a greater chance of buckle initiation in the next thermal cycle. The onset of infilling is marked in Fig. 4. A dependency on particle size is seen, and is discussed later. Once infilling begins, the frequency at which slope failures and load spikes occur is higher in fine sand, reflecting the smaller displacement at which the finer particles fall around the pipe.

Deformation Mechanisms

Fig. 5 shows Test CD at various stages of upward pipe displacement, δ. The peak uplift resistance was mobilized at a displacement of 2.95 mm ($\delta_p=1\%H$), which is in close agreement with the literature (Trautmann et al. 1985; Bransby et al. 2001). At this stage, a small circular gap was open beneath the pipe. The gap

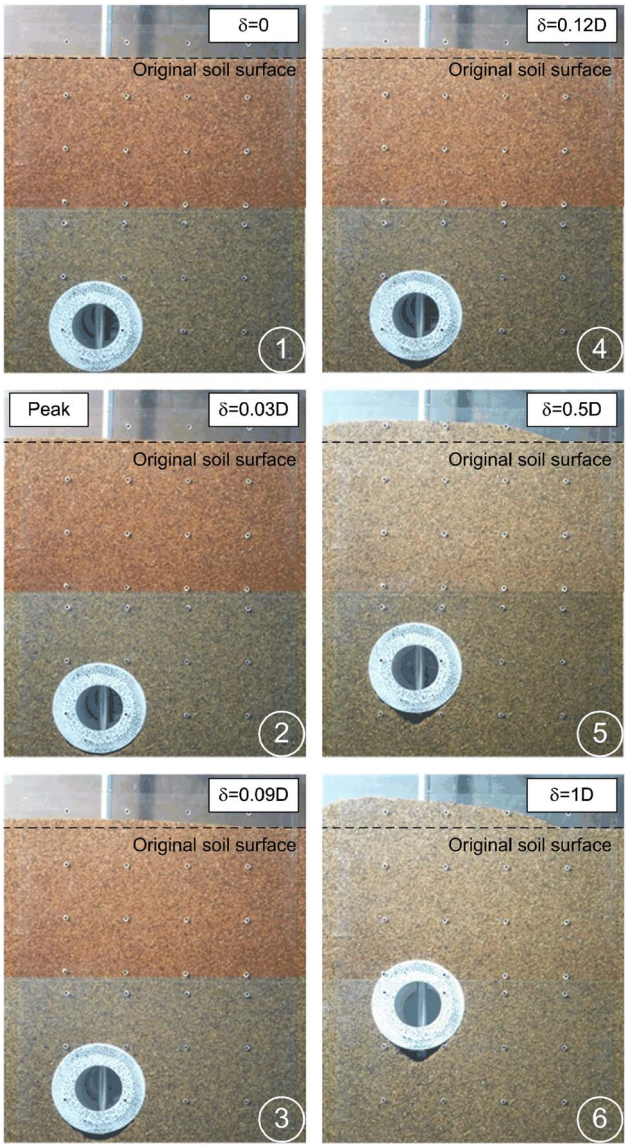

Fig. 5. Change in soil geometry during pipe uplift in dense coarse sand (Test CD)

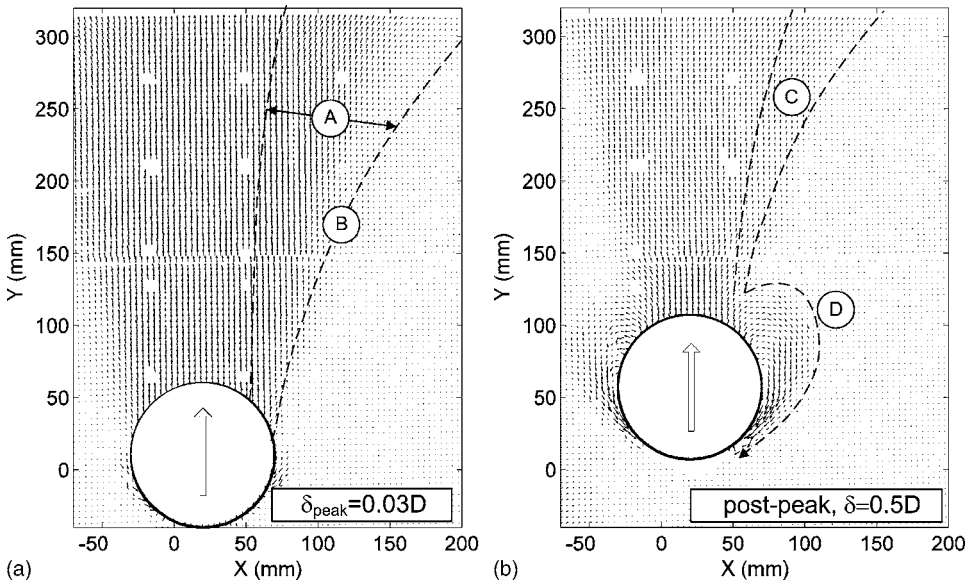

Fig. 6. Displacement field in dense coarse sand (Test CD): (a) At peak resistance; (b) at a pipe displacement of 0.5 D

grew and the side slopes straightened due to infilling. The side slopes were straight by a pipe displacement of ~12 mm and the shape of the cavity remained constant thereafter. The dilatant behavior of the dense soil caused significant surface heave at larger pipe displacements. The net dilation of the soil is evident from the greater surface heave compared with the cavity underneath the pipe.

Fig. 6 shows the displacement fields calculated in Test CD at peak resistance and at a pipe displacement of 0.5*D*. The vectors in the figures represent the incremental displacements (i.e., the instantaneous velocities) normalized by the upward pipe movement between the two images under consideration, and are scaled up by a factor of 5 for clarity. At peak resistance, wide zones of distributed shear are evident (A), rather than velocity jumps (i.e. shear planes). The zones of shear are inclined and curve outwards (B), indicating increasing dilation towards the ground surface, where the stress level is lower. Similar curved failure surfaces have been observed in model tests by Stone and Newson (2006). Downward soil movement is evident near the pipe shoulders. After peak resistance is mobilized, the shear zones become narrower and more vertical (C), as the shear strain localizes and dilation ends. Also, the narrow sliding block is accompanied by a flow-around mechanism leading to downward soil movement around the pipe shoulders (D).

The results of Test CD suggest that the deformation mechanism during pipe uplift consists of four key stages:

1. Mobilization of peak resistance.
2. Onset of infilling beneath the pipe invert.
3. Postpeak shear band formation.
4. Flow around.

All these mechanisms are observed in the other three tests. Nevertheless, the behavior varies from one test to another, depending on the particle size and soil density. The detailed mechanisms at various stages are compared in the following.

Mobilization of Peak Uplift Resistance

Fig. 7 shows the horizontal profiles of vertical movement at peak resistance. Each curve represents the vertical component of the incremental soil displacement at the corresponding level above the pipe. The profiles have been normalized by the incremental pipe displacement and scaled so the pipe velocity corresponds to 50 mm.

In all tests the deformation mechanism resembles an inverted trapezoidal block, bounded by distributed shear zones curving outwards and widening towards the surface. For coarse sand, the width of the shear zone near the pipe crown is about 40 mm irrespective of the soil density, while that of fine sand is about 20 mm. The influence of soil density can be seen in the soil movement near the ground surface. For the two dense models (Tests CD and FD), the ground movement is about 90% of the

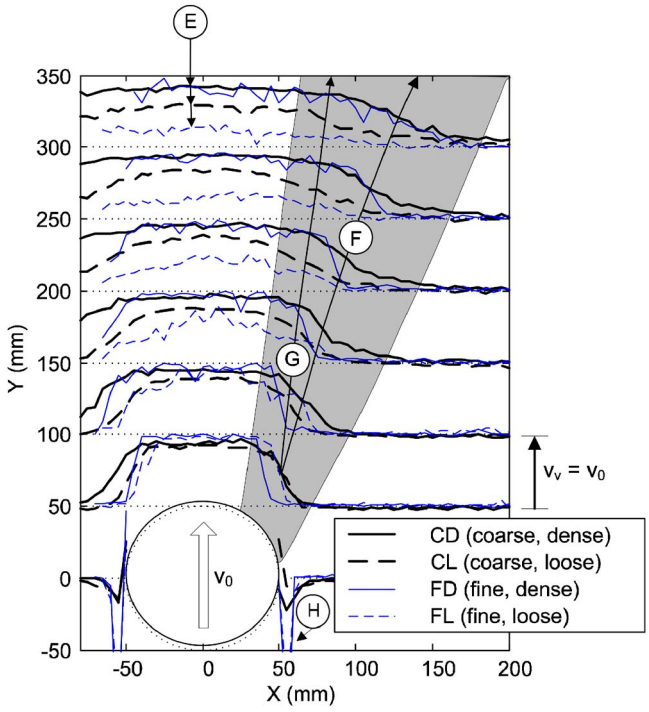

Fig. 7. Vertical movement profiles at peak resistance

pipe displacement, reflecting the higher stiffness and dilatancy of the soil column (E). The ground movement in the two loose models (Tests CL and FL) is less.

The inclination of the distributed shear zone is influenced by density. As shown in Fig. 7, the shear zone mobilized in the dense coarse sand (F) has a greater inclination angle to the horizontal compared to that of loose coarse sand (G). The lines labeled (F) and (G) delineate the shear zone by passing through the points at which the vertical velocity is half the value above the centerline. For fine sand, the distributed shear zone in the dense model (Test FD) also has a greater inclination angle than that in the loose model (Test FL). This is evident by the large upward soil movement remote from the centerline near the surface ($X=100$ mm, $Y=300$ mm), where the loose model shows negligible movement. The average inclination of the distributed shear zone for dense sand is about 16 and 20° to the vertical for coarse and fine sand respectively, whereas values for loose soil are about 10 and 6°, respectively. These angles are defined by drawing a straight line passing through a point on the lowest vertical soil velocity profile above the pipe and another point on the highest velocity profile. These two points are the locations at which the vertical velocity is half the value above the centerline at that level.

The dilation angle is difficult to identify since the shearing is distributed and the shear zone is curved, but it is clear from the average inclination of the shear zone that the soil is not dilating at an angle equal to the peak mobilized friction angle, which must be equal to or exceed the critical state value of 32°, so normality is violated. A prediction method that faithfully replicates the peak uplift mechanism must assume that $\phi \neq \psi$. Consequently, it is unavoidable that some assumption must be made about the shear resistance on the slip planes, in order to calculate this component of resistance.

The magnitude of this additional shearing resistance can be estimated from the deformation mechanism in Fig. 7. From vertical equilibrium of the uplifting soil, this shearing resistance is equal to the uplift resistance, minus the weight of the trapezoid of soil contained within the shear zones. Using the derived average dilation angles of 18 and 8° for the dense and loose tests respectively, the weight of the lifted soil is 75 and 49 N in each case (Table 2). These values are labeled on Fig. 4 as trapezoid weight, and show that shearing resistance accounts for approximately 40% of the peak uplift resistance in both cases.

In these four tests, the mobilization distance for peak resistance, δ_P, is unaffected by density or particle size, with the values agreeing within 10% (Table 2). This observation eliminates D_{50} as a dimension by which to normalize the mobilization displacement, leaving the pipe diameter, D, and the embedment depth, H. Both of these parameters are likely to influence δ_P as follows. There is a smooth horizontal profile of vertical velocity near the ground surface at peak resistance (Fig. 7). The strain rate at a point in this zone depends on the local gradient of this velocity profile, which is linked to the vertical movement divided by the width of the profile—and therefore the pipe movement divided by the diameter. Also, as the vertical velocity varies with distance above the pipe (Fig. 7), a greater pipe movement would be necessary to mobilize the strength of a greater depth of cover. So, both δ/D and δ/H are relevant dimensionless variables. Finite element analyses by Bransby et al. (2001) show that only δ/H matters, whereas experimental results by Trautmann et al. (1985) show that both D and H influence δ_P. As only density and grain size were varied in this study, it can only be concluded that these parameters have negligible influence, although it can be noted

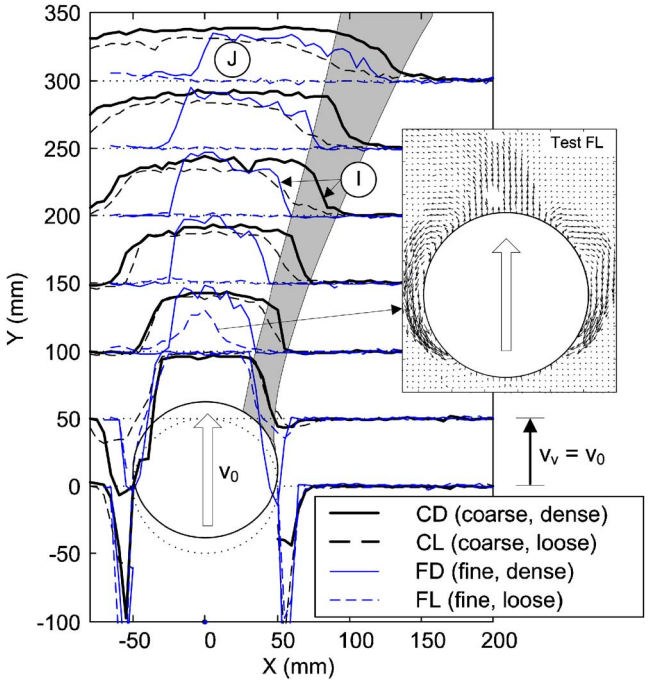

Fig. 8. Vertical movement profiles at a pipe displacement of 0.12 D

that the measured values of $\delta_P/D=3\%$ and $\delta_P/H=1\%$ are in broad agreement with those reported by previous authors.

Infilling Mechanism

The postpeak softening of the load–displacement response is due to (1) the onset of infilling below the pipe invert, which reduces the need to lift soil above the pipe and (2) a reduction in the mobilized friction on the shear planes above the pipe, as the soil moves from peak to critical state. Infilling contributes to the onset of irreversible uplift, since the pipe cannot fall back to the original position.

The onset of infilling depends on grain size. The velocity profiles at peak resistance showed significant downward soil movement adjacent to the pipe shoulders in fine sand but not in coarse sand (marked as H in Fig. 7). This downward movement is soil falling around the periphery of the pipe and infilling below the pipe invert via a slope failure. In the fine sand, this infilling mechanism begins at the same moment as peak resistance is mobilized. In the coarse sand, inspection of the images show that no infilling occurred until a pipe movement of 9 mm. Fig. 8 shows the velocity profiles of the four tests at a pipe displacement of 12 mm. In both fine and coarse sand, infilling is evident from the large downward displacement near the pipe shoulders in all the tests.

These observations indicate that the onset of infilling is dependent on grain size, although not in linear proportion. In the tests on fine sand, infilling begins at a displacement of 3 mm, or $10D_{50}$. In coarse sand, infilling commences after a pipe movement of 9 mm, or $4D_{50}$.

Shear Band Formation and Flow around

Fig. 8 also shows evidence of shear band formation above the pipe. Comparison of the shaded areas in Figs. 7 and 8—which bound the shear zones—shows that the shear band width reduces

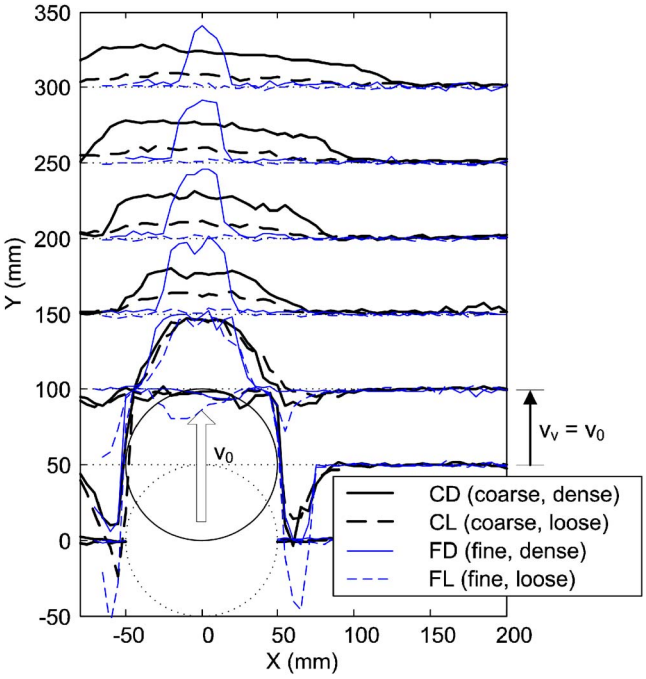

Fig. 9. Vertical movement profiles at a pipe displacement of 0.5 D

postpeak. In dense sands, the velocity profiles have near-vertical jumps, indicating that the deformation is concentrated into plane (I).

As the soil close to the pipe shoulders can now fall downwards, the uplifting block becomes narrower. Also, beyond peak, dilation is reduced and the uplifting block is steeper sided. In the case of fine loose sand, no heave is evident at the ground surface (J), and the mechanism is entirely confined close to the pipe—as shown by the inset in Fig. 8. This flow-around mechanism, with a triangular soil wedge ahead of the pipe, is mobilized at a displacement of 12 mm, or 0.12*D*. This distance is likely to scale with pipe diameter, *D*, as the flow-around mechanism is independent of the free surface so is unlikely to be related to cover depth, *H*. The flow-around mechanism in loose fine sand is more local to the pipe than in dense coarse sand [Fig. 6(b)], reflecting the more contractile behavior.

The transition from primarily heave of a soil block, to primarily flow-around continues as the pipe is displaced further. This change is progressive, with no distinct transition evident. It is not possible to identify whether this transition is better linked to pipe diameter, or to grain size. The triggering of infilling around the pipe periphery has some grain size dependency.

Fig. 9 shows the velocity profiles in all tests at a pipe displacement of 50 mm (i.e., 0.5*D*). Combined heave and flow around is observed, except for the loose fine soil, in which no heave is observed. The rate of surface heave is approximately half of that seen in Fig. 8 (at $\delta = 12$ mm), reflecting less dilation, and flow-around instead of lifting of the soil.

Fig. 10 shows the instantaneous velocity fields close to the pipe at $\delta = 50$ mm. The flow-around mechanism is not symmetri-

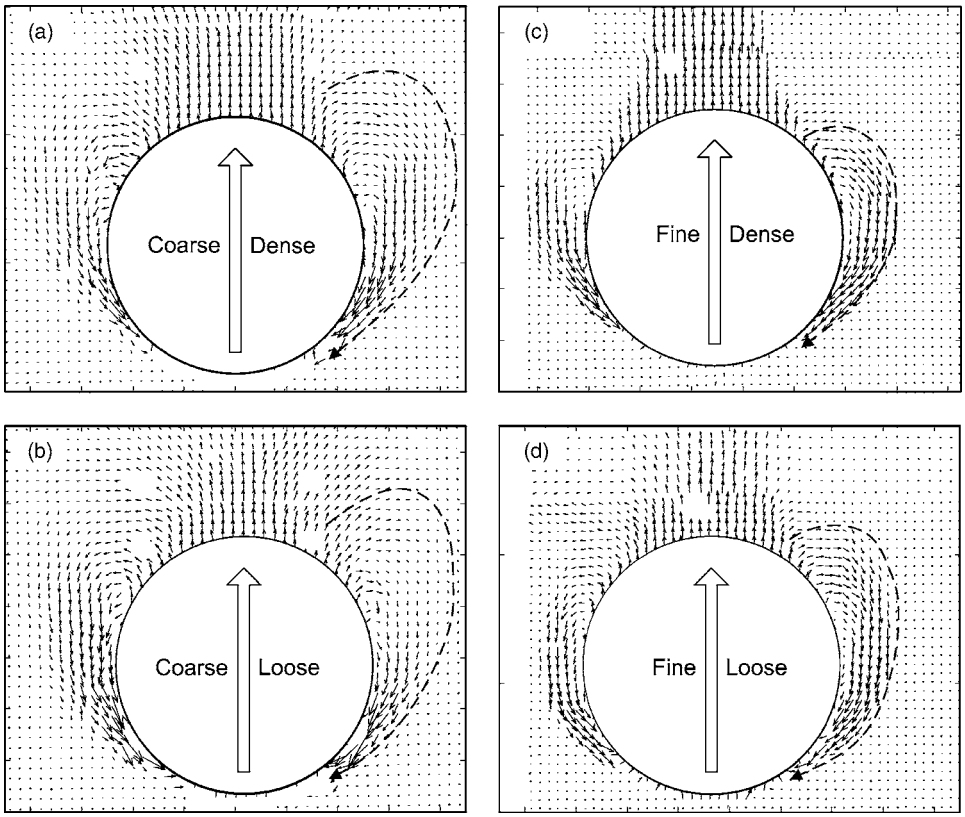

Fig. 10. Flow-around mechanism at a pipe displacement of 0.5 D: (a) Dense coarse sand (Test CD); (b) loose coarse sand (Test CL); (c) dense fine sand (Test FD); and (d) loose fine sand (Test FL)

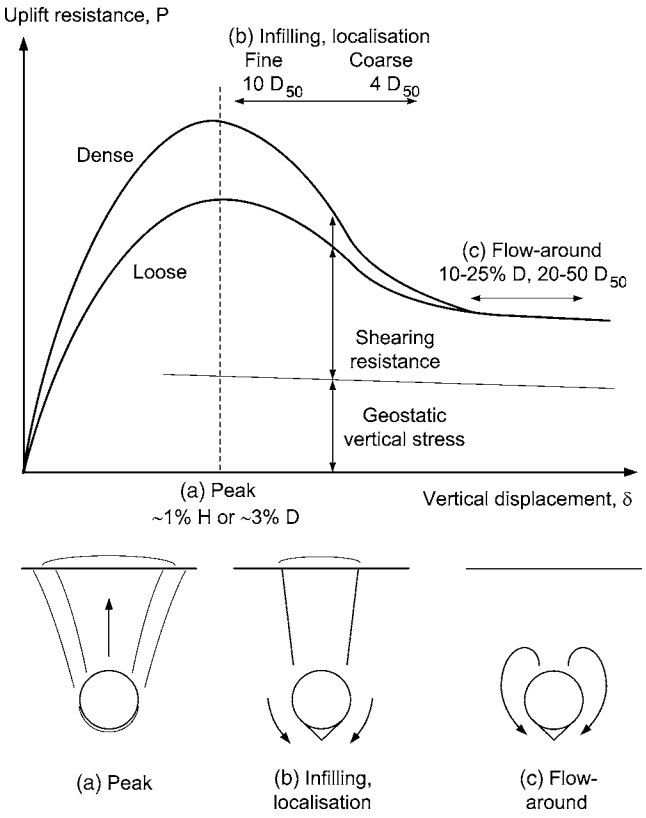

Fig. 11. Summary of uplift load-displacement response and the corresponding deformation mechanisms

cal about the horizontal axis of the pipe, as is the case for plasticity solutions for flow around a cylinder in clay (Randolph and Houlsby 1984). Instead, this flow-around mechanism has a vertical velocity at the pipe crown, to satisfy symmetry, then circulates through approximately 240° (i.e., 180+60°) to end with gravity-driven slope failure into the cavity beneath the pipe at an inclination of around 30° to the horizontal. In fine sand [Figs. 10(c and d)] the flow-around mechanism is more confined than in coarse sand [Figs. 10(a and b)], reflecting the thinner, but more regular landslides triggered by the smaller particles.

Implications for the Prediction of Peak Uplift Resistance

The deformation mechanisms observed during these tests are summarized in Fig. 11 and have the following implications for predicting uplift resistance:

1. Peak resistance is associated with the formation of a sliding block bounded by a pair of distributed dilating shear zones. Normality is not obeyed, so prediction methods for peak uplift resistance based on associated flow do not capture the operative mechanism. Comparison of the measured uplift resistance and the observed weight of lifted soil indicates that shearing resistance with a vertical component is mobilized within the shear zones.
2. Since normality is violated, the limit equilibrium method can represent the failure mechanism better than a strict plasticity upper bound by accommodating different angles of friction and dilation. However, a limit equilibrium solution requires the distributed shear zones to be idealized as shear planes and some assumed flow rule to link friction and dilation angles with some assumed distribution of stress along the shear planes.

These conclusions allow the realism of the mechanisms assumed by each prediction method (Fig. 1) to be evaluated. The vertical slip model [Fig. 1(b)] does not correctly capture the deformation at peak resistance. Of the solutions based on inclined planes [Fig. 1(c)], the strict upper bound ($\phi=\psi$) overestimates the dilation and therefore the width of the lifted soil block. The two limit equilibrium solutions (Vermeer and Sutjiadi 1985; White et al. 2001) capture more closely the actual inclination of the shear zones, by using Rowe, 1962 and Bolton's (1986) flow rules, respectively. However, these solutions necessarily idealize the distributed shear zones as planes. A more detailed comparison of the measured and predicted values of uplift resistance in these tests, and a database of other published uplift tests is contained in a companion paper.

Conclusions

The deformation mechanisms during uplift of pipes buried in silica sand have been studied by image analysis. Four stages have been identified: peak resistance, infilling, shear band formation and flow around.

For both dense ($I_D=\sim 90\%$) and loose ($I_D=\sim 30\%$) sands, the peak uplift resistance is mobilized through the formation of a rigid soil block bounded between a pair of distributed shear zones. The shear zones curve slightly outward due to higher dilatancy near ground surface. The average inclination of the shear zones is influenced by the soil density, with denser soil being more dilatant. The magnitude of the peak uplift resistance is unaffected by particle size for the chosen cover depth-to-diameter ratio. However, the width of the shear zones is strongly dependent on grain size.

The movement required to mobilize peak uplift resistance is independent of particle size and soil density for the chosen test conditions. A cavity with sloping sides forms beneath the pipe during the mobilization of peak resistance. For the fine sand, particles begin to infill this cavity after $\sim 10D_{50}$ of pipe movement, leading to irrecoverable upward pipe displacements. For the coarse sand, this infilling mechanism occurs at a later stage at a pipe displacement of $\sim 4D_{50}$.

After peak resistance, the shear strain concentrates into a pair of narrow shear bands, then a flow-around mechanism is formed accompanied by a reduction in the uplift resistance. The rate of shear band formation decreases with an increase in particle size.

Of previously proposed prediction models, a limit equilibrium solution assuming an inclined shear surface best describes the operative mechanism during pipe uplift. However, this approach requires an assumption of the shear resistance on the slip surfaces, which are simplified from distributed shear zones. As normality is not observed, a strict upper bound using associated flow is not appropriate.

In this study, the deformation mechanism has been observed at only one particular buried depth of $H/D=3$, which is typical of offshore pipelines. This behavior, especially the mobilization displacements, may change with embedment depth. Further studies are required to address this uncertainty.

References

Bolton, M. D. (1986). "The strength and dilatancy of sands." *Geotechnique*, 36(1), 65–78.

Bransby, M. F., Newson, T. A., Brunning, P., and Davies, M. C. R. (2001). "Numerical and centrifuge modeling of the upheaval resistance of buried pipelines." *Proc., 20th Int. Conf. on Offshore Mechanics and Arctic Engineering*, Rio de Janeiro, Brazil.

Cheuk, C. Y. (2005). "Soil-pipeline interaction at the seabed." Ph.D. dissertation, Univ. of Cambridge, Cambridge, U.K.

Chin, E. L., Craig, W. H., and Cruickshank, M. (2006). "Uplift resistance of pipelines buried in cohesionless soil." *Proc., 6th Int. Conf. on Physical Modelling in Geotechnics*. Ng, Zhang, and Wang, eds., Vol. 1, Taylor & Francis Group, London, 723–728.

Cousens, T. W. (1980). "The gravity flow of bulk solids in bunkers." Ph.D. dissertation, Univ. of Cambridge, Cambridge, U.K.

Dickin, E. A. (1994). "Uplift resistance of buried pipelines in sand." *Soils Found.*, 34(2), 41–48.

Hooper, J., Maschnes, E., and Farrant, T. (2004). "Penguin pipeline system—Design challenges for the world's longest snaked lay HP/HT PIP tie-back." *Offshore Pipeline Technology Conf.*, Amsterdam, The Netherlands.

Lee, S. Y. (1989). "Centrifuge modeling of cone penetration testing in cohesionless soils." Ph.D. dissertation, Univ. of Cambridge, Cambridge, U.K.

Mak, K. W. (1983). "Some centrifugal test results on the grain size effect in physical modelling." *Geotechnical Group Technical Rep. No. 140*, Cambridge Univ. Engineering Dept., Cambridge, U.K.

Ng, C. W. W., and Springman, S. M. (1994). "Uplift resistance of buried pipelines in granular materials." *Centrifuge 94*, Leung, Lee, and Tan, eds., 753–758.

Randolph, M. F., and Houlsby, G. T. (1984). "The limiting pressure on a circular pile loaded laterally in cohesive soil." *Geotechnique*, 34(4), 613–623.

Rowe, P. W. (1962). "The stress-dilatancy relation for static equilibrium of an assembly of particles in contact." *Proc. R. Soc. London, Ser. A*, 269, 500–527.

Schaminée, P. E. L., Zorn, N. F., and Schotman, G. J. M. (1990). "Soil response for pipeline upheaval buckling analyses: Full-scale laboratory tests and modeling." *Proc., 22nd Annual Offshore Technology Conf., OTC6486*, 563–572.

Schupp, J., Byrne, B. W., Eacott, N., Martin, C. M., Oliphant, J., Maconochie, A., and Cathie, D. (2006). "Pipeline unburial behaviour in loose sand." *Proc., 25th Int. Conf. on Offshore Mechanics and Arctic Engineering*, Hamburg, Germany, OMAE2006-92541.

Stone, K. J. L., and Newson, T. A. (2006). "Uplift resistance of buried pipelines: An investigation of scale effects in model tests." *Proc., 6th Int. Conf. on Physical Modelling in Geotechnics*, Ng, Zhang, and Wang, eds., Vol. 1, Taylor & Francis Group, London, 741–746.

Stroud, M. A. (1971). "Sand at low stress levels in the simple shear apparatus." Ph.D. dissertation, Univ. of Cambridge, Cambridge, U.K.

Take, W. A. (2003). "The influence of seasonal moisture cycles on clay slopes." Ph.D. dissertation, Univ. of Cambridge, Cambridge, U.K.

Trautmann, C. H., O'Rourke, T. D., and Kulhawy, F. H. (1985). "Uplift force-displacement response of buried pipe." *J. Geotech. Engrg.*, 111(9), 1061–1076.

Vanden Berghe, J. F., Cathie, D., and Ballard, J. C. (2005). "Pipeline uplift mechanisms using finite element analysis." *Proc., 16th Int. Conf. of Soil Mechanics and Foundation Engineering*, Osaka, Japan, 1801–1804.

Vermeer, P. A., and Sutjiadi, W. (1985). "The uplift resistance of shallow embedded anchors." *Proc., of 11th Int. Conf. of Soil Mechanics and Foundation Engineering*, Vol. 3, San Francisco, 1635–1638.

White, D. J. (2002). "An investigation into the behaviour of pressed-in piles." Ph.D. dissertation, University of Cambridge, Cambridge, U.K.

White, D. J., Barefoot, A. J., and Bolton, M. D. (2001). "Centrifuge modeling of upheaval buckling in sand." *Int. J. Physical Modeling in Geotechnics*, 2(1), 19–28.

White, D. J., Randolph, M. F., and Thompson, B. (2005). "An image-based deformation measurement system for the geotechnical centrifuge.." *Int. J. Physical Modeling in Geotechnics*, 5(3), 1–12.

White, D. J., Take, W. A., and Bolton, M. D. (2003). "Soil deformation measurement using particle image velocimetry (PIV) and photogrammetry." *Geotechnique*, 53(7), 619–631.